Identifying reproducible macroscopic traffic patterns in a year-long data set

Lukas Ambühl
IVT, ETH Zurich
CH-8093, Switzerland
Tel: +41 44 633 32 51
Email: ambuehll@ethz.ch

Allister Loder*
IVT, ETH Zurich
CH-8093, Switzerland
Tel: +41 44 633 62 58
Email: aloder@ethz.ch

Ludovic Leclercq
Univ. Lyon, ENTPE, IFSTTAR, LICIT
UMR_T 9401, F-69518, LYON, France
Tel: +33 4 72 04 77 16
Email: ludovic.leclercq@entpe.fr

Kay W. Axhausen
IVT, ETH Zurich
CH-8093, Switzerland
Tel: +41 44 633 39 43
Email: axhausen@ethz.ch

Monica Menendez
Division of Engineering, New York University Abu Dhabi
Tandon School of Engineering, New York University
IVT, ETH Zurich
Tel: +971 2 628 5273
Email: monica.menendez@nyu.edu

* Corresponding author

Paper submitted for presentation at the 98th Annual Meeting Transportation Research Board, Washington D.C., January 2019

Word count: 4268 words + 1 table(s) × 250 + 500 (references) = 5018 words

May 9, 2024

ABSTRACT

The macroscopic Fundamental Diagram (MFD) provides a novel perspective on urban traffic that facilitates new policies and strategies to cope with recurring congestion. The MFD is assumed to be well-defined and reproducible, but, so far, no long-term empirical evidence for this shape assumption exists. In this paper, we use an extensive one-year traffic data set from Lucerne, recent advances in modeling the MFD shape as well as established similarity measures (Dynamic time warping and Fréchet distance) and k-medoid clustering to investigate this assumption. We first find that we can reduce the complexity of urban traffic throughout the year to only three or five clusters depending on the selected similarity measure. Furthermore, we reveal that the MFD shape in the loading phase of the network is very similar across the observed inflow patterns over the course of a year, but less so for the unloading and full-day MFD.

Keywords: MFD Similarity Congestion Cluster

INTRODUCTION

There is a growing evidence that human mobility patterns in cities follow laws and recurring patterns (1, 2, 3), that - not surprisingly - result in recurring congestion patterns (4, 5, 6, 7, 8). Using the appropriate tools, such patterns allow the accurate prediction of traffic states and travel times for journey planners (9, 10, 11, 12). Among the tools used, the recently introduced macroscopic fundamental diagram (MFD) provides a paradigm shift, which consist in moving our attention from minimizing travel times to maximizing the overall number of trips (13). The MFD itself describes with a well-defined and reproducible curve the relationship between the accumulation of vehicles and the travel production in vehicle kilometers in an urban network. Importantly, each MFD has at the network's critical vehicle accumulation a distinct maximum of travel production.

So far, the daily MFD has not been investigated over a long time period. In other words, the reproducibility of the MFD has only been established for short time periods. Closing this gap is important because the MFD shape results from a complex interplay between network topology, signal settings (14, 15), routes, demand (16), and public transport interactions (17, 18), i.e. bridging the traffic demand and supply side. Proof for the existence of a long-term reproducibility is key to the concept of the MFD, as it allows to simplify urban traffic in an unprecedented way for macroscopic applications, ranging from traffic control (19), to pricing (20) and the allocation of urban space (21).

Existing empirical MFD work suggests that indeed the MFD shape is reproducible across a number of days, especially during the loading phase of the network, (22, 23, 24, 25, 26). Unfortunately until now, a lack of longitudinal empirical data as well as methodology to measure MFD pattern similarity and subsequently clustering prevented a detailed analysis for longer time periods. In this paper, we use advances in modeling the MFD's shape (27) combined with established sequence similarity measures to identify daily MFD patterns and to quantify the MFD's reproducibility over the course of a year using empirical data from Lucerne, Switzerland. In the field of the MFD research, the closely related term *partitioning* already exists for identifying homogeneous sub-regions in networks (28, 29, 30), but our research focuses on the overall MFD shape across days and its temporal clustering, instead of the spatial distribution of vehicle densities within a day.

This paper presents the first empirical evidence on the reproducibility of the MFD shape and a methodology to analyze MFD patterns for long periods of time (i.e. one year). Depending on the methodology measuring the similarity of MFD patterns, we observe only three or five global clusters of MFD patterns. We find that they can be classified by day of week and average total inflow. For all non-weekend clusters, we find that the MFD's shape in the network loading phase is most similar across demand clusters, while the MFD shapes are less similar for the recovery phase. These findings confirm not only the reproducibility of the MFD's shape, but also increase the validity of models built around the MFD.

The remainder of this paper is organized as follows. The next section introduces the similarity measures for MFD patterns as well as clustering in the context of the MFD. We then introduce the empirical data set used, before presenting the results of the clustering and shape reproducibility analysis. The paper ends with discussion and conclusions.

ANALYZING MFD PATTERNS

Measuring similarities in patterns

In our analysis, we consider the MFD as a joint time-series of flow $q(t)$ and density $k(t)$ over the course of the day. This joint time-series does not only describes the resulting MFD of the considered day, but also captures the aggregate dynamics of network loadings and recoveries that result from the overall demand. This perspective is particularly useful to address the question of how many daily MFD patterns can be observed over time in an empirical context, and whether we can link the different MFD shapes to certain observable traffic aspects. So far, in the literature, MFD patterns in time-sequences have not been analyzed.

In mathematical terms, the similarity σ between sequences $a(t)$ and $b(t)$ can be expressed by

$$\sigma(a(t), b(t)) = \Gamma[a(t), b(t)] \tag{1}$$

where Γ describes the function returning the similarity measure, or in a physical analogy the distance between $a(t)$ and $b(t)$. The most common similarity or distance measure between two sequences is the Euclidean distance. In its simplest approach according to Eqn. 2, at each time instance t the Euclidean distance between sequence $a(t)$ and $b(t)$ is computed and subsequently summed up over all time periods of an observation period (day, week, month).

$$\Gamma_{Euclid}[a(t), b(t)] = \sum_{t=1}^{T} \sqrt{\sum_{i=1}^{N} (a_i(t) - b_i(t))^2} \tag{2}$$

Figure 1a shows this behavior for the MFD, where the distance between the two MFDs is measured for every point in time. The bars in this figure correspond to the measured distance. Especially for $t = 4$ and $t = 6$ the temporal mismatch in the pattern creates a substantial distance. Arguably, this approach is very strict and penalizes even a temporal mismatch between sequences at the smallest temporal resolution, which might not be desired in the context of the MFD. For example, if a highly similar loading of the network starts with a five minute difference between two days, they will not be considered similar by this measure although they exhibit a similar pattern.

Therefore, we consider and compare two other approaches for Γ that are more flexible in the time dimension: *dynamic time warping* (DTW) (31, 32) and the Frechét distance (FRE) (33). Although their primary field of application are one-dimensional time series, using the Euclidean distance allows a straightforward extension to multi-dimensional time-series as the MFD. In the next two subsections we briefly introduce these two approaches. For the computation of the similarity measures, we use the software provided by (34).

Dynamic time warping

In contrast to comparing the distance between sequences at the same time, DTW deforms the time axis in both $a(t)$ and $b(t)$ within allowed limits to analyze the similarity. This procedure is looking for a warping path W where element w_k aligns the elements $a(i)$ and $b(j)$ so that their distance δ, here Euclidean, is minimized. The warping paths require some mathematical constraints, e.g. monotonicity, continuity and a warping window for time mismatch between i and j (further mathematical explanations can be found in (31)). In mathematical terms, DTW searches for the warping path W that is minimizing the cumulative distance between sequences $a(t)$ and $b(t)$ as indicated by Eqn. 3.

$$\Gamma_{DTW}[a(t), b(t)] = \min_{W} \left(\sum_{k=1}^{P} \delta(w_k) \right) \tag{3}$$

Figure 1b illustrates the MFD case for the DTW problem, where the procedure is assigning *new* time values (indicated by a prime) based on the warping paths along which the distance is minimized. Arguably, this feature of DTW is very useful for MFD patterns as network loading and recovery must not start or end at the same time, even if they maintain a similar shape. Nevertheless, this similarity measure requires the definition of a physical meaningful warping window, and this is not necessarily trivial.

Frechét distance

The meaning and interpretation of the Frechét distance is best introduced with a very popular example: Let us think about a girl walking her dog. The girl walks on one trajectory while the dog walks on another trajectory. Both can vary their speed, even stop, but are not allowed to go back in time. The Frechét distance is the minimal length of the leash required for completing the walk.

In mathematical terms, Eqn. 4 describes this problem. $a(i)$ is re-parameterized to a $(\alpha(\tau))$ to map from the unit interval, and similarly for b. For further mathematical insights we refer the reader to previous work by (33).

$$\Gamma_{FRE}\left[a(t), b(t)\right] = \inf_{\alpha,\beta} \max_{\tau\in[0,1]} \left\{\delta\left(a(\alpha(\tau)), b(\beta(\tau))\right)\right\} \tag{4}$$

Figure 1c depicts the idea of the Frechét distance in the MFD context, where the leash corresponds to the bar that links both MFDs. The algorithm searches for the shortest required line linking both MFD patterns. This algorithm does not require a minimum warping window as DTW (window can be set to infinity if physically meaningful and computational resources are available), and might be able to uncover slightly more differences in pattern than DTW. The Frechét optimization problem is computationally exhaustive compared to DTW, making it more difficult to work with in large scale empirical contexts.

Clustering

In general, the clustering or partitioning of data can be divided into two overarching classes: supervised and unsupervised clustering. Here, we will focus on the implementation of unsupervised approaches (35).

Further, we use *k-medoid* or *k-median* clustering (36, 37). We select this approach over the more common *k-means* algorithm because the *k-medoid* partitions around an element (medoid or median) of the sample. In the context of the MFD, each cluster is assigned one medoid MFD that is representative for its cluster and thus can be interpreted and analyzed. This is not possible with *k-means*. Another advantage of *k-medoid* is the possibility to evaluate the similarity of each object within its cluster and to its neighboring clusters visually with the silhouette plot (38), assessing the cluster's coherence and variation. The silhouette value is always in the range of -1 to 1 and is attributed to each member of a cluster. A value close to 1 indicates that a particular day is well matched to its corresponding cluster, whereas a value close to -1 indicates that the chosen cluster is a poor match. The average silhouette over all members indicates the overall quality of the clustering. For clustering, we use the R package by (39).

Clustering of MFD shapes has been done previously using heuristics (25). However, this approach is only a rough quantification of the MFD shape, but does not allow for statistical testing and does not account for dynamic influences (40).

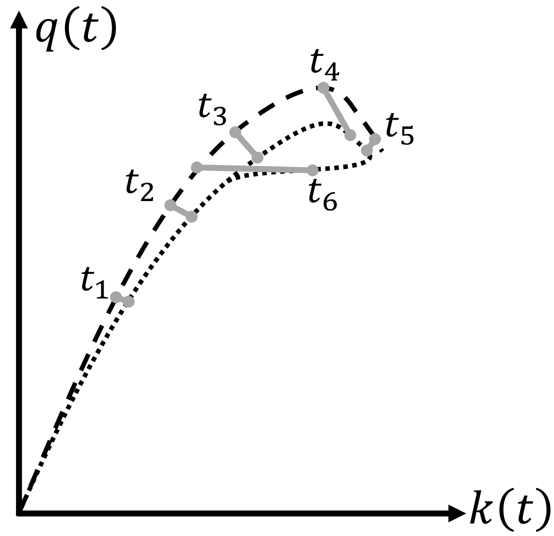

(a) Euclidian

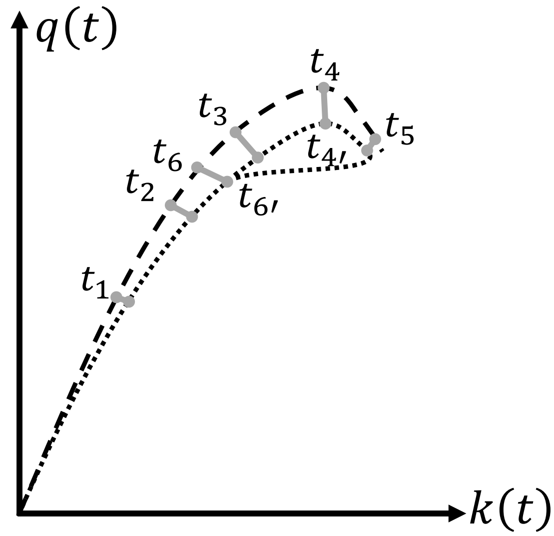

(b) DTW

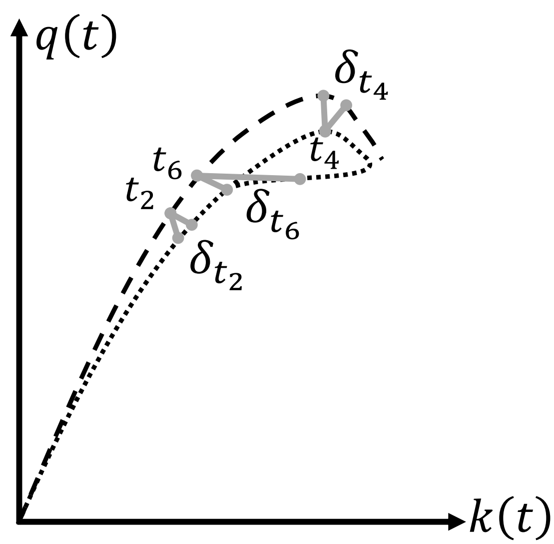

(c) Fréchet

FIGURE 1 : MFD representation of similarity measures.

Measuring MFD shape similarity

In order to answer the question to what extent the MFD is well-defined and reproducible, we have to measure and quantify the MFD shape. For this, we use recent advances by (27), where the authors propose a single parameter functional form for the MFD. This single parameter function requires the analytical definition of an upper MFD (uMFD), e.g. a simple trapezoidal shape with parameters derived using the methodology by (14). The uMFD is time-invariant and is based on the fundamental diagram of the individual streets, traffic control, and the capacity of an average intersection. It is therefore a rough first order approximation of the MFD and serves as a reference MFD. Eqn. 5 shows the function where k is the density, $v(k)$ is the speed MFD, and u_f, Q, κ and w are the trapezoidal shape parameters (u_f is the free flow speed, Q is the average link capacity, κ is the jam density, and w is the backward wave speed). These parameters can easily be obtained from actual measurements and from local authorities. For quantifying the actual MFD shape, only the parameter λ has to be estimated from the daily speed MFD with non-linear least squares.

$$v(k) = -\lambda \ln\left(\exp\left(-\frac{u_f k}{\lambda}\right) + \exp\left(-\frac{Q}{\lambda}\right) + \exp\left(-\frac{(\kappa - k)w}{\lambda}\right)\right)/k \tag{5}$$

λ measures how far the observed MFD is located from the uMFD. The larger λ, the farther away the observed MFD is located from the uMFD. In case the MFD shape is reproducible and well-defined, λ should take the same value for each and every day.

DATA

For this analysis, we use a longitudinal MFD data set from the city of Lucerne, Switzerland, spanning the entire year 2015. In total, we use data from 352 days in the year 2015. 13 days are excluded as they clearly showed irregular behavior due to too many missing loops, system breakdowns, or special events. The MFDs are recorded from inductive loop detectors located upstream and downstream of intersections. Figure 2a shows a map of Lucerne with the locations of all detectors marked. We first filter all defective measurements and smooth the 3min measurements with a moving average technique. Further, we ensure that only a single detector per lane is used for MFD estimation. The MFD is estimated using a common technique for stationary traffic sensors (41). As the distribution of loop detectors across the length of the link is rather uniform, we do not account for a potential placement bias in the MFD.

As loop detectors measure only flow and occupancy, but not density, we need to adjust the MFD to measure density and thus in turn average space-mean speed in the network. We adjust the MFD by identifying the fastest hour in the MFD, typically in the morning or evening, before or after rush hour when the network is only slightly loaded. For this hour, we then query the Google routes API for 1000 random trips through Lucerne, and then match the speed distribution from the MFD in the fastest hour with the speed distribution of the API query to obtain the adjustment scalar. The adjusted MFD for Lucerne is then given in Figure 2b.

RESULTS

In the following, we discuss the results of the MFD pattern clustering, once measuring the similarity with dynamic time warping (DTW) and once with the Fréchet distance (FRE). We denote each cluster with the previous mentioned abbreviation for the similarity measure, followed by the cluster number. In general, we observe highly similar clustering outcomes for the two different similarity measures, where the Fréchet distance seems to be able to retain slightly more informa-

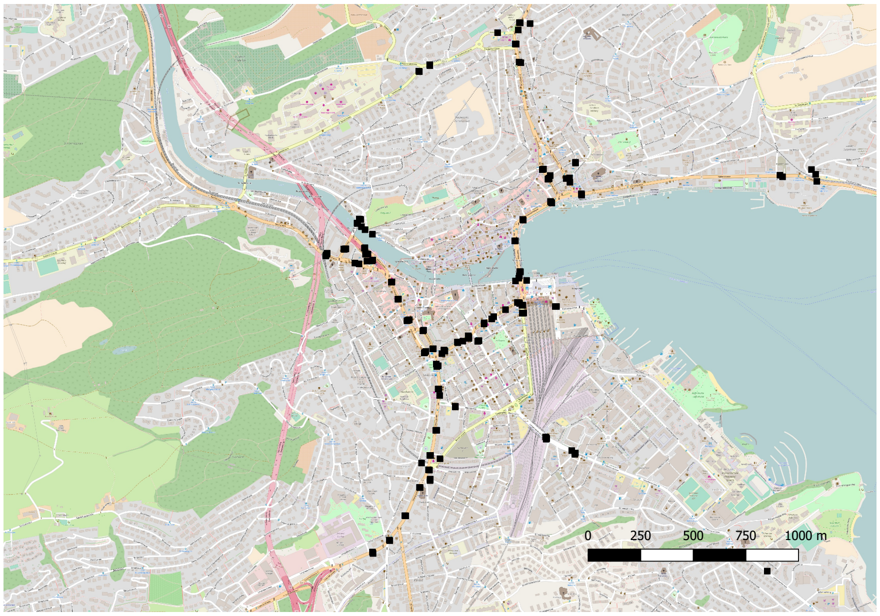

(a) City map of Lucerne with the location markings of the detectors.

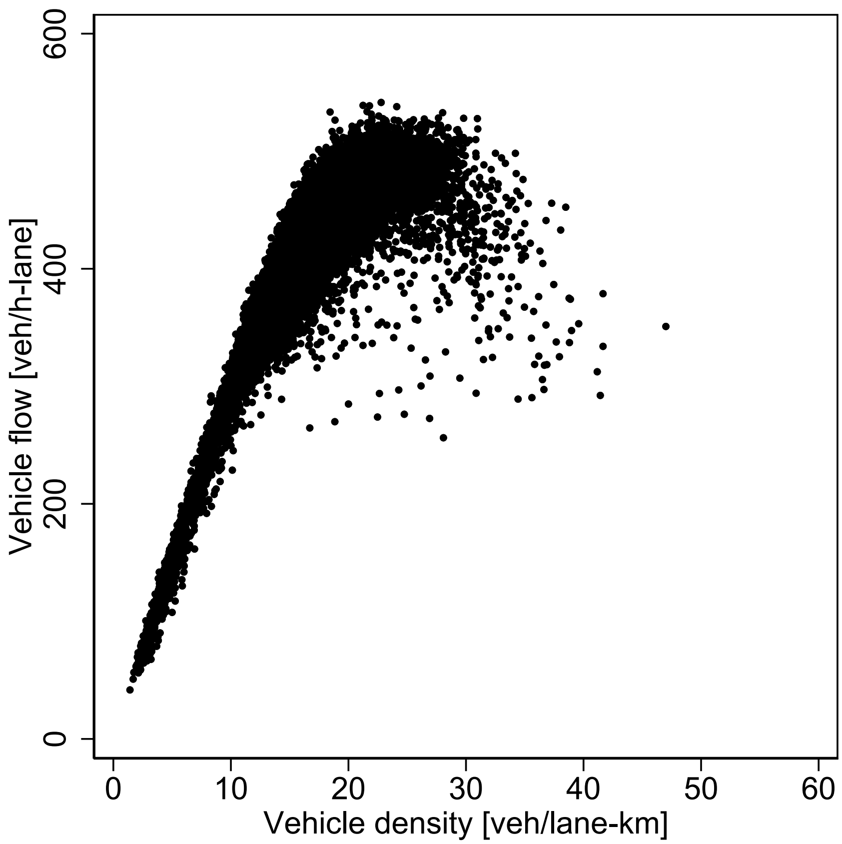

(b) Full year MFD of Lucerne (352 days)

FIGURE 2 : Information on the empirical data used for this analysis.

tion than DTW. We will first investigate the general form of the MFD over the course of a full day and try to reveal differences between the clusters found. Afterwards, we will analyze in more details the MFDs' loading and recovery phases.

In Figure 3 we show the results for the one-year data of Lucerne for which we find that the average silhouette value is maximized for DTW with two clusters, while for Fréchet three clusters are needed. Recall that a silhouette value closer to 1 indicates a high similarity of a daily MFD pattern to the cluster, whereas a value closer to -1 means a poor match. The resulting silhouette plots are shown for DTW in Figure 3a and for Fréchet in Figure 3b. The colour of each day represents whether it is a weekend day or not. First, we find that all weekends are located in DTW1 (117 days) as well as FRE1 (89 days) and FRE2 (28 days), while DTW2 (235 days) and FRE3 (235 days) only contain weekdays. Thus, we define the first group as the weekend clusters, while the latter group are the weekday clusters. Further investigation of the type of days shows that FRE2 covers mostly Sundays and public holidays. Second, we find that the silhouette distribution within each cluster exhibit a different shape. Especially for DTW, we see that the weekday cluster is more robust, i.e. has more similar days, as expressed with a less steep decline in silhouette values as in the weekend cluster. This seems intuitive, as on weekdays car drivers might be less flexible in terms of activity and departure time choices compared to weekends, not mentioning all special events that often place on weekends.

As the *k-medoid* clustering methodology returns the most representative member of each cluster as the so-called medoid, we show these medoids in Figure 3c and 3d, as well as the MFDs of all days attributed to each cluster. At first sight we find that the medoids are located well within each cluster, emphasizing the idea of the medoid being a good representative of that cluster. In both, Figure 3c and 3d, we see the expected loading pattern based on the previous Figures 3a and 3b: DTW1, FRE1 and FRE2 show a lower loading on a typical weekend day compared to DTW2 and FRE3, where traffic is even found to be in the congested regime. However, it becomes clear from Figure 3d that the difference between FRE1 and FRE2 is not in terms of the general MFD shape, but must be located in the temporal evolution of the MFD. This emphasizes that the similarity measures not only capture the MFD's shape, but also the temporal aspects of the MFD. For a better understanding of the clusters, we further show the time series of the average flows and speeds for the respective medoids in Figures 3e and 3f. Clearly, the average flow is different for DTW1 and DTW2 during the morning hours. Furthermore, DTW1 almost always shows higher speeds than DTW2. Similarly, the weekend clusters FRE1 and FRE2 exhibit a later loading of the network and higher speeds than FRE3.

As the weekend cluster seems to be sufficiently determined by the type of day, we further concentrate on the higher loaded weekday clusters and investigate them with a second level clustering. Therefore, we perform another clustering for the 234 days of DTW2 and FRE3. The clustering results in two clusters for DTW with DTW2.1 (108 days) and DTW2.2 (126 days) and three clusters for Fréchet with FRE3.1 (52 days), FRE3.2 (104 days) and FRE3.3 (78 days). Again, we present the silhouette plots in Figures 4a and 4b as well as the medoids in Figures 4c and 4d. Colours in the silhouette plot represent the different days of the week. Interestingly, we find that cluster DTW2.1 is more likely to occur at the beginning of the week, while cluster DTW2.2 is more likely to be observed at the end of the week. The results for Fréchet show a similar behavior, FRE3.2 seems to more or less describe the mid-week conditions, while FRE3.1 (beginning of week) and FRE3.3 (end of week) follow the behavior observed for DTW. This distinction might not be surprising as Switzerland, including Lucerne, is known to have many weekly commuters,

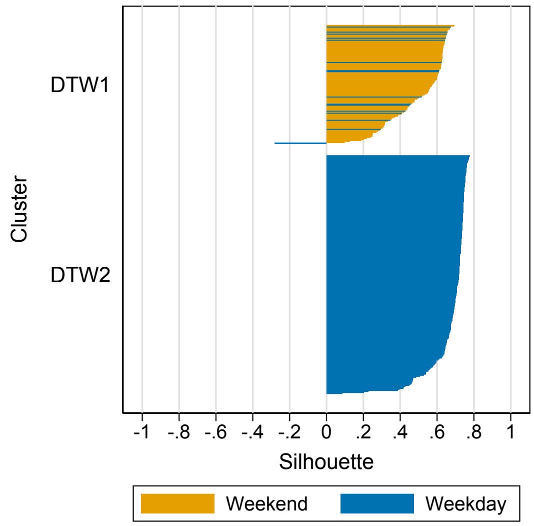

(a) Silhouette plot for DTW measure.

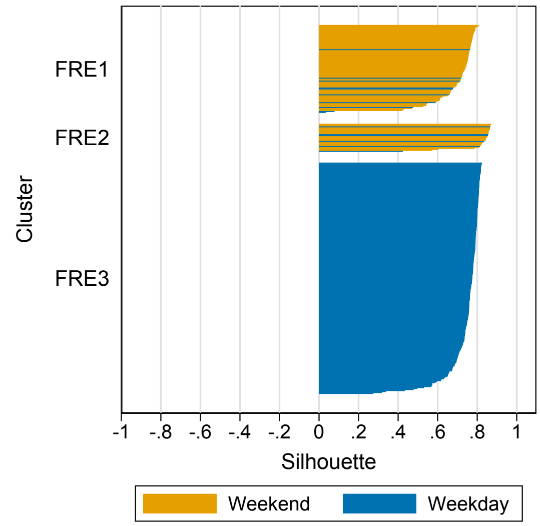

(b) Silhouette plot for Fréchet measure.

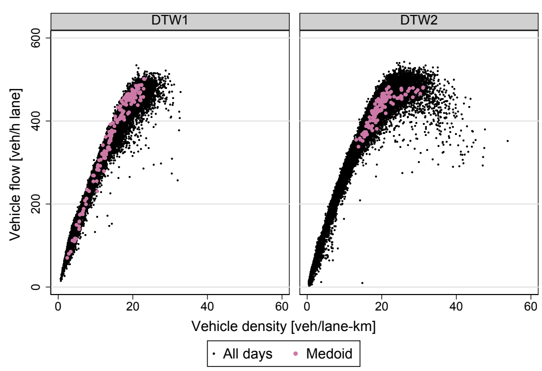

(c) All MFDs and medoids for DTW.

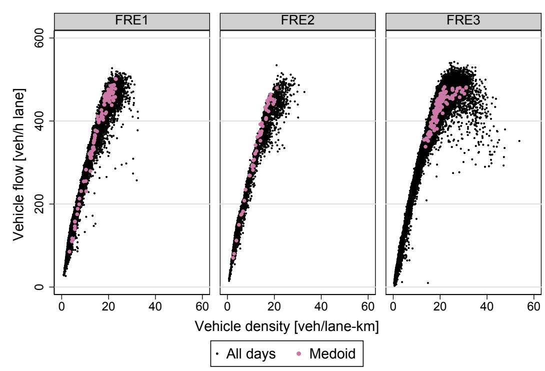

(d) All MFDs medoids plot for Fréchet.

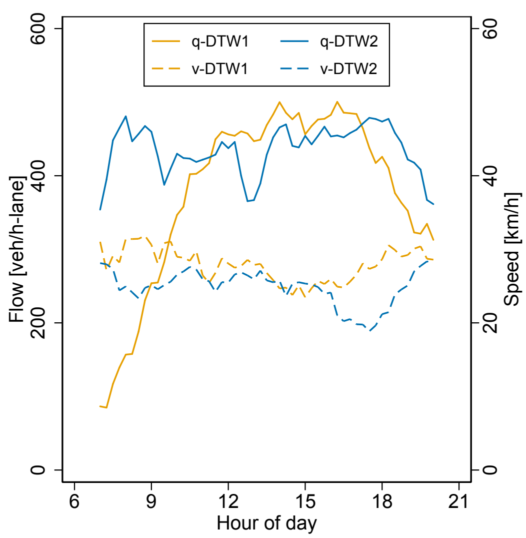

(e) Average flows and speeds of the medoids for DTW.

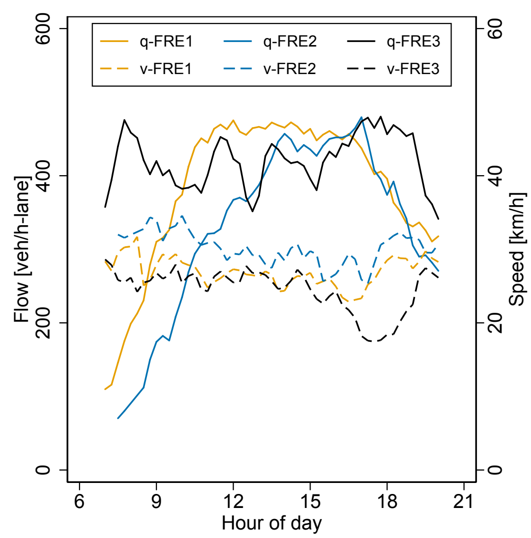

(f) Average flows and speeds of the medoids plot for Fréchet.

FIGURE 3 : First level clustering results.

where we can expect different OD demands at the beginning of the week from those at the end of the week. Second, the silhouette values are on average lower and exhibit a steeper slope for the DTW2 and FRE3 clusters (see also Figure 3), showing that the now recovered clusters show less within-cluster similarity than before. This is intuitive as the clustering algorithm is now scrutinizing the differences within the normal weekday pattern.

The medoids in Figures 4d and 4c reveal mostly a distinction between a normal weekday pattern without indication of a congested branch (DTW2.1, FRE3.1), and with indication of a congested branch (DTW2.2, FRE3.2, FRE3.3). Given that this is the second level of clustering, it makes sense that the differences between the cluster medoids' average speed and flow shown in Figures 4e and 4f are less accentuated than in the first level. Nonetheless, we can observe certain differences, in particular between FRE3.1, FRE3.2 and FRE3.3, where morning speeds are lowest for FRE3.2, contrary to evening speeds that are lowest for FRE3.3. A potential reason why Fréchet distinguishes between the very similar FRE3.1 and FRE3.2 can be seen in Figure 5 that shows the cumulative inflows into the city for the medoid days. Here, we observe that FRE3.2 has more inflow throughout the day than FRE3.1, even though both result in a similar medoid without congestion. At the same time, we see that FRE3.3 exhibits some congestion for the same level of inflow as FRE3.2.

Based on the similarity measure, we identified three (DTW) and five (Fréchet) clusters in our one year data set for the city of Lucerne that capture not only the shape of the MFD, but also the overall inflow into the city throughout the day. We now further investigate the differences between the found clusters by estimating the shape defining parameter λ as introduced by (27) for each day in the data set, as well as for the loading and unloading phase separately. We identify the loading and unloading phases in the network by decomposition of the density time series into a seasonal and trend component. From the latter component, we identify network loading in a time interval when the trend is increasing, and a network unloading when the trend is decreasing. In other words, it is possible that there are multiple loading and unloading phases during a day. DTW and the Fréchet clusters are only meaningful, when applied to continuous time series. Given the fact that there are potentially multiple loading and unloading phases during a single day - interrupting the time series - we refrain from applying the clustering to the loading and unloading phases separately, but estimate λ for each sample. Nonetheless, it is still possible to investigate the robustness of the initially found clusters with respect to their loading and unloading behaviour.

In Figure 6 we show the kernel density plots of λ for every cluster, during the full day, the loading, and the unloading phase, respectively. For the weekday clusters, we find that for all analyzed cases the distributions overlap to a large extent. We test for similarity of the distributions using the two-sample Kolmogorov-Smirnov test. Table 1 shows the pairings of clusters the loading and unloading phase of the MFD, respectively. The values for full day MFD are included for completeness, but we focus on the loading and the unloading phases. The p-value indicates the probability to observe the two randomly sampled distributions drawn from the same population, i.e. the smaller the value the more likely it is that the two samples are not from the same distribution. Despite the relatively broad distribution of λ, we conclude that in the loading phase of the network, all considered combinations show a non-zero chance of being from the same population - even for different inflow scenarios, e.g. FRE3.1 and FRE3.3, we obtain MFDs of similar shape. This supports the notion that relatively small changes in the demand do not affect the shape of the MFD substantially. The p-value decreases for the full day MFD as well as the unloading phase to more or less zero, except for the combination FRE3.1 and FRE3.3 that shows in all three cases a non-zero

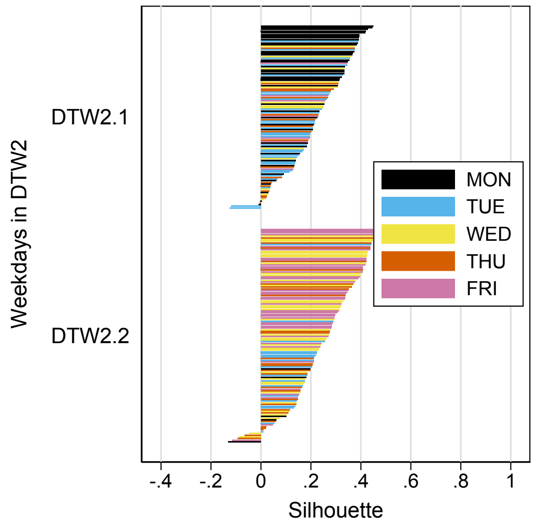

(a) Silhouette plot for DTW.

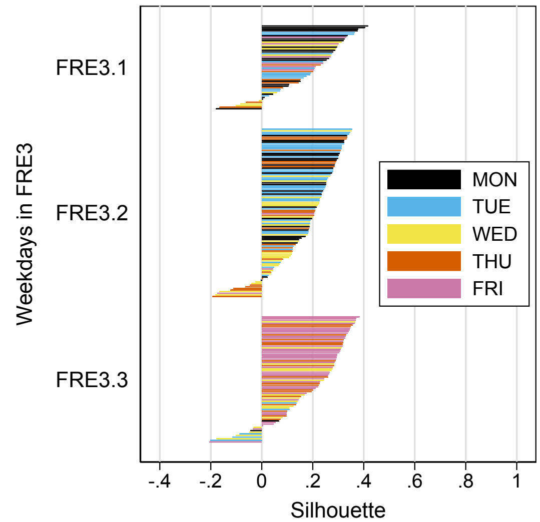

(b) Silhouette plot for Fréchet.

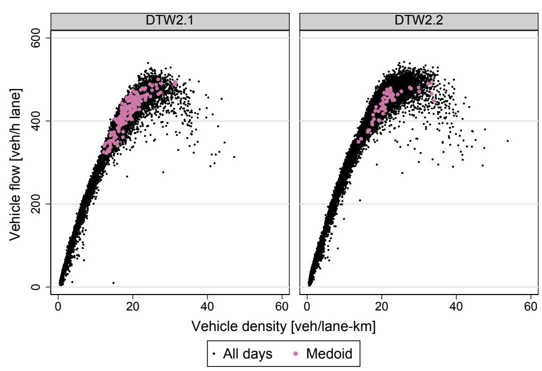

(c) All MFDs and medoids for DTW.

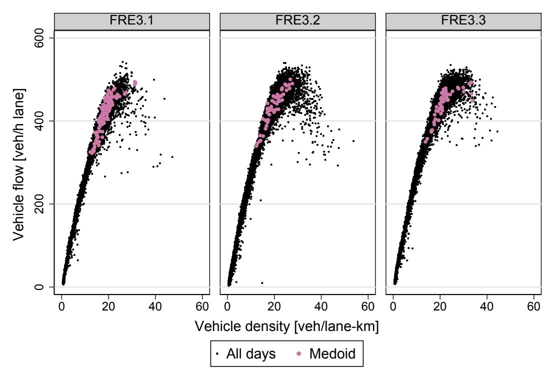

(d) All MFDs and medoids for Fréchet.

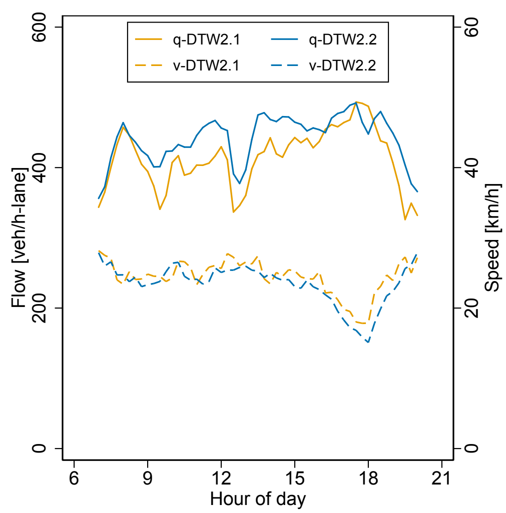

(e) Average flows and speeds of the medoids for DTW.

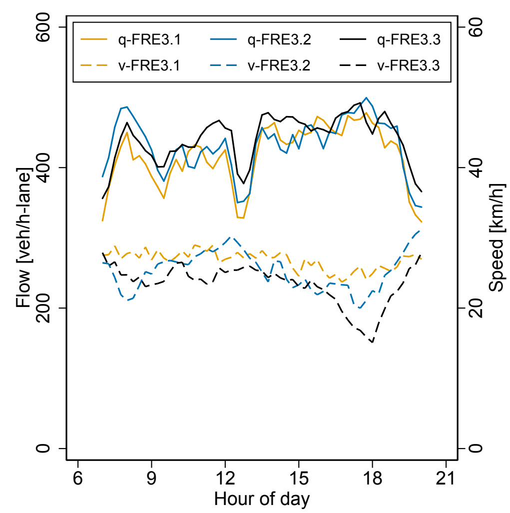

(f) Average flows and speeds of the medoids for Fréchet.

FIGURE 4 : Second level clustering results.

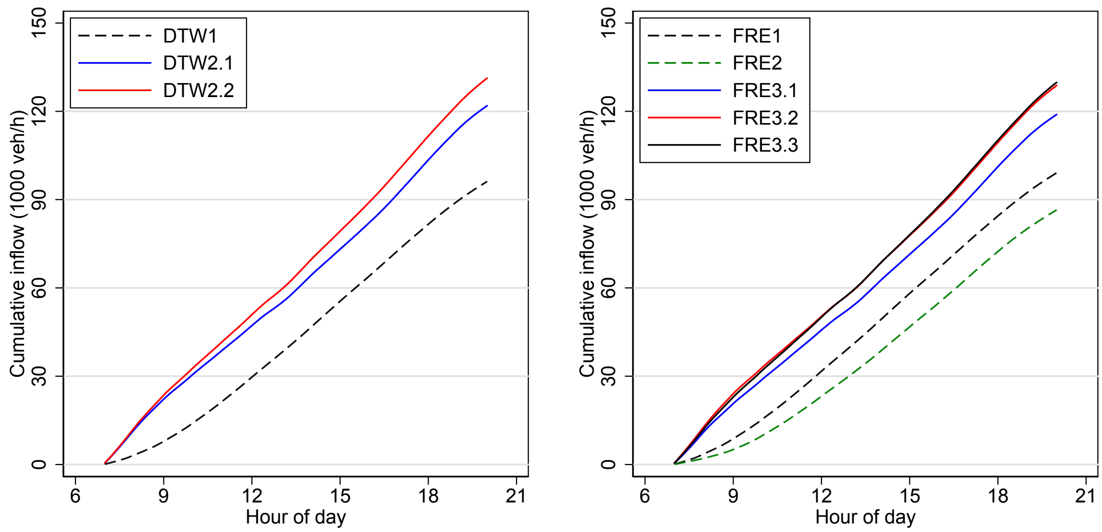

(a) DTW clusters. (b) Fréchet clusters.

FIGURE 5 : Reservoir inflows for the medoid MFDs.

value, i.e. they are less likely to be from the same distribution. These findings are reasonable, as the unloading of the traffic network is known to be more heterogeneous than its loading. In other words, unloading the network can follow many different paths in an MFD, contrary to the loading. Such differences can result in hysteresis effects, as investigated previously by (40). However, in the relatively small network, we observe only thirteen days with a substantial hysteresis, all clustered in DTW2 and FRE3. At the second level clustering, these days are then distributed across all clusters.

As the *k-medoid* clustering algorithm returns a representative element for each cluster as the median or medoid element, we can further analyze whether these medoids have statistically significant different λ. Therefore, we estimate for each medoid in the second clustering level λ and the corresponding 95 % confidence interval. We find both for DTW and Fréchet overlapping confidence intervals, except when comparing FRE3.1 with FRE3.2 and FRE3.3. However, in those cases we find that the difference is not significantly different from zero.

It is clear that the found clusters and interpretations are context-specific to Lucerne, but the results emphasize the power of the proposed MFD pattern similarity measures to reveal congestion patterns within a city. Furthermore, the city of Lucerne might be comparatively small in relation to larger cities, such as Singapore or Los Angeles where congestion levels might be more severe and more MFD patterns might be present. Nevertheless, the results show that we can reduce the complexity of one year traffic into a hand full of representative clusters, where cluster membership can be determined by day of week as well as average city inflow. A general implication from these findings is that the assumption of a relatively well-defined and, in particular, reproducible MFD is indeed satisfied.

DISCUSSION AND CONCLUSIONS

In this paper we address the question whether the MFD's shape is reproducible over a long time period. Using an extensive one-year traffic data set, we find that we can reduce the daily MFD

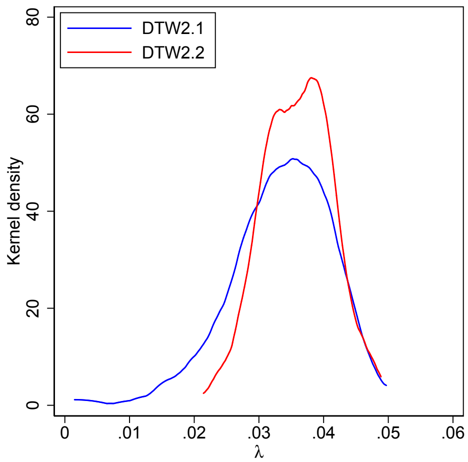

(a) Full day MFD, DTW.

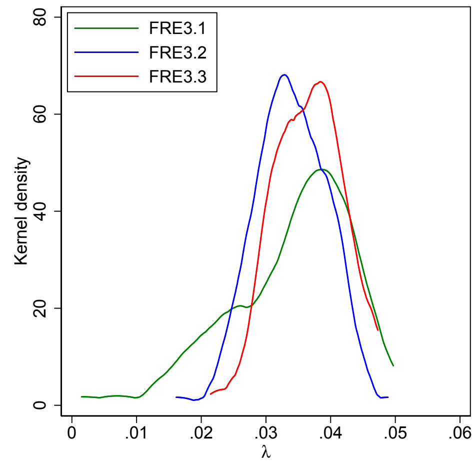

(b) Full day MFD, Fréchet.

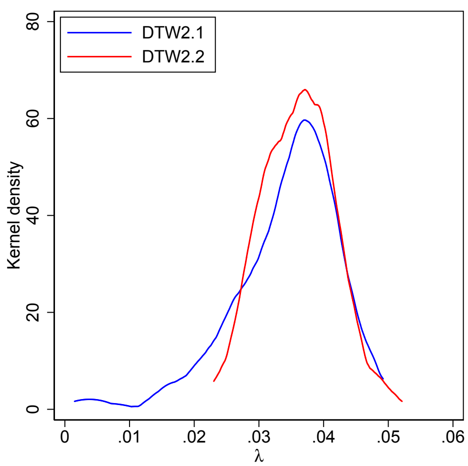

(c) Loading MFD, DTW.

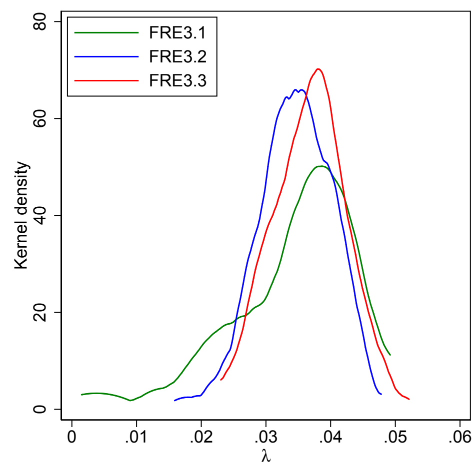

(d) Loading MFD, Fréchet.

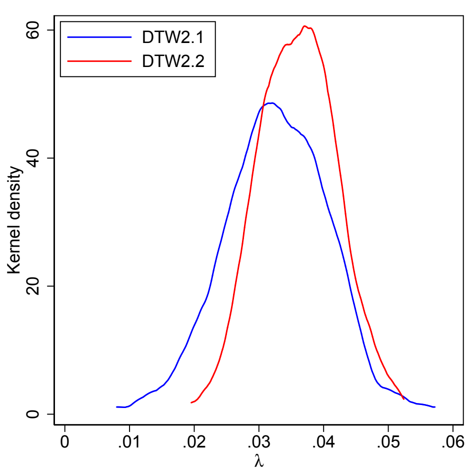

(e) Unloading MFD, DTW.

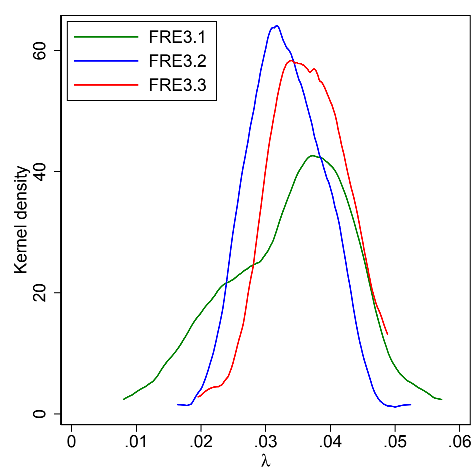

(f) Unloading MFD, Fréchet.

FIGURE 6 : Distributions of λ grouped by the identified clusters. λ is calculated using non-linear least squares with uMFD parameters: $u_f = 7.4$ m/s , $Q = 0.177$ veh/s,$w = 2.1$ m/s, and $\kappa = 0.135$ veh/lane-km.

Full day MFD		p-value
DTW2.1	DTW2.2	0.043
FRE3.1	FRE3.2	0.131
FRE3.1	FRE3.3	0.392
FRE3.2	FRE3.3	0.032
Loading		
DTW2.1	DTW2.2	0.218
FRE3.1	FRE3.2	0.397
FRE3.1	FRE3.3	0.318
FRE3.2	FRE3.3	0.106
Unloading		
DTW2.1	DTW2.2	0.003
FRE3.1	FRE3.2	0.005
FRE3.1	FRE3.3	0.284
FRE3.2	FRE3.3	0

TABLE 1 : Summary of *p*-values from the two-sample Kolmogorov-Smirnov for each pair of weekday clusters.

patterns into only three or five clusters depending on the methodology used for measuring the MFD pattern's similarity. Interestingly, we see that the top-level clusters differentiate between weekends and public holidays, and weekdays. Even though the performance of complex urban traffic networks depends on many factors, including travel demand, traffic control, route choice, and interactions between different traffic modes, the findings presented show that the observed patterns are reproducible day after day. We further showed that certain differences can partially be explain by the inflow into the city.

The city of Lucerne does not compare to the large metropolises around the globe and thus we cannot generalize to more complex networks. Nevertheless, our methods allow an in-depth analysis with data from metropolises, so that this question can be answered in a more generalized way.

Our results also align with previous research about human travel behavior that revealed some repetitive patterns. Interestingly, the small set of clusters and our ability to explain cluster membership also has its implications for traffic state and travel time predictions: By knowing the type of day, the average reservoir inflow and the current time of day, we can estimate the space-mean speed with reasonable accuracy. In conclusion, the proposed procedure for clustering MFD patterns is very promising to understand urban congestion.

AKNOWLEDGEMENTS

This work was supported by ETH Research Grants ETH-04 15-1 and ETH-27 16-1 and has received funding from the European Research Council (ERC) under the European Union's Horizon 2020 research and innovation program (grant agreement No 646592 – MAGnUM project). We would like to thank Thomas Karrer and Milena Scherer from the City of Lucerne for their support

and providing the data.

AUTHOR CONTRIBUTION STATEMENT

The authors confirm contribution to the paper as follows: study conception and design: Lukas Ambühl, Allister Loder; data collection: Lukas Ambühl, Allister Loder; analysis and interpretation of results: Lukas Ambühl, Allister Loder, Ludovic Leclercq, Monica Menendez; draft manuscript preparation: Allister Loder, Lukas Ambühl, Ludovic Leclercq, Monica Menendez, K.W. Axhausen. All authors reviewed the results and approved the final version of the manuscript.

References

[1] González, M. C., C. A. Hidalgo, and A. L. Barabasi, Understanding individual human mobility patterns. *Nature*, Vol. 453, No. 7196, 2008, pp. 779–82.

[2] Noulas, A., S. Scellato, R. Lambiotte, M. Pontil, and C. Mascolo, A tale of many cities: universal patterns in human urban mobility. *PLoS One*, Vol. 7, No. 5, 2012, p. e37027.

[3] Sun, L., K. W. Axhausen, D.-H. Lee, and X. Huang, Understanding metropolitan patterns of daily encounters. *Proceedings of the National Academy of Sciences*, Vol. 110, No. 34, 2013, pp. 13774–13779.

[4] Lopez, C., L. Leclercq, P. Krishnakumari, N. Chiabaut, and H. van Lint, Revealing the day-to-day regularity of urban congestion patterns with 3D speed maps. *Scientific Reports*, Vol. 7, No. 1, 2017, p. 14029.

[5] Wang, P., T. Hunter, A. M. Bayen, K. Schechtner, and M. C. González, Understanding road usage patterns in urban areas. *Scientific Reports*, Vol. 2, 2012, p. 1001.

[6] Louf, R. and M. Barthelemy, How congestion shapes cities: from mobility patterns to scaling. *Scientific Reports*, Vol. 4, 2014, p. 5561.

[7] Louail, T., M. Lenormand, M. Picornell, O. Garcia Cantu, R. Herranz, E. Frias-Martinez, J. J. Ramasco, and M. Barthelemy, Uncovering the spatial structure of mobility networks. *Nature communications*, Vol. 6, 2015, p. 6007.

[8] Colak, S., A. Lima, and M. C. González, Understanding congested travel in urban areas. *Nature communications*, Vol. 7, 2016, p. 10793.

[9] Mori, U., A. Mendiburu, M. Álvarez, and J. A. Lozano, A review of travel time estimation and forecasting for Advanced Traveller Information Systems. *Transportmetrica A: Transport Science*, Vol. 11, No. 2, 2015, pp. 119–157.

[10] Stathopoulos, A. and M. G. Karlaftis, A multivariate state space approach for urban traffic flow modeling and prediction. *Transportation Research Part C: Emerging Technologies*, Vol. 11, No. 2, 2003, pp. 121–135.

[11] van Lint, J. W. C., S. P. Hoogendoorn, and H. J. van Zuylen, Accurate freeway travel time prediction with state-space neural networks under missing data. *Transportation Research Part C: Emerging Technologies*, Vol. 13, No. 5-6, 2005, pp. 347–369.

[12] Chun-Hsin, W., H. Jan-Ming, and D. T. Lee, Travel-time prediction with support vector regression. *IEEE Transactions on Intelligent Transportation Systems*, Vol. 5, No. 4, 2004, pp. 276–281.

[13] Daganzo, C. F., Urban gridlock: Macroscopic modeling and mitigation approaches. *Transportation Research Part B: Methodological*, Vol. 41, 2007, pp. 49–62.

[14] Daganzo, C. F. and N. Geroliminis, An analytical approximation for the macroscopic fundamental diagram of urban traffic. *Transportation Research Part B: Methodological*, Vol. 42,

2008, pp. 771–781.

[15] Leclercq, L. and N. Geroliminis, Estimating MFDs in simple networks with route choice. *Transportation Research Part B: Methodological*, Vol. 57, 2013, pp. 468–484.

[16] Leclercq, L., C. Parzani, V. L. Knoop, J. Amourette, and S. P. Hoogendoorn, Macroscopic traffic dynamics with heterogeneous route patterns. *Transportation Research Part C: Emerging Technologies*, Vol. 59, 2015, pp. 292–307.

[17] Boyaci, B. and N. Geroliminis, Estimation of the network capacity for multimodal urban systems. *Procedia - Social and Behavioral Sciences*, Vol. 16, 2011, pp. 803–813.

[18] Castrillon, F. and J. Laval, Impact of buses on the macroscopic fundamental diagram of homogeneous arterial corridors. *Transportmetrica B: Transport Dynamics*, Vol. in press, 2017, pp. 1–16.

[19] Haddad, J. and N. Geroliminis, On the stability of traffic perimeter control in two-region urban cities. *Transportation Research Part B: Methodological*, Vol. 46, 2012, pp. 1159–1176.

[20] Zheng, N., R. A. Waraich, N. Geroliminis, and K. W. Axhausen, A dynamic cordon pricing scheme combining a macroscopic and an agent-based traffic model. *Transportation Research Part A: Policy and Practice*, Vol. 46, 2012, pp. 1291–1303.

[21] Zheng, N. and N. Geroliminis, On the distribution of urban road space for multimodal congested networks. *Transportation Research Part B: Methodological*, Vol. 57, 2013, pp. 326–341.

[22] Geroliminis, N. and C. F. Daganzo, Existence of urban-scale macroscopic fundamental diagrams: Some experimental findings. *Transportation Research Part B: Methodological*, Vol. 42, 2008, pp. 759–770.

[23] Loder, A., L. Ambühl, M. Menendez, and K. W. Axhausen, Empirics of multi-modal traffic networks – Using the 3D macroscopic fundamental diagram. *Transportation Research Part C: Emerging Technologies*, Vol. 82, 2017, pp. 88–101.

[24] Buisson, C. and C. Ladier, Exploring the Impact of Homogeneity of Traffic Measurements on the Existence of Macroscopic Fundamental Diagrams. *Transportation Research Record: Journal of the Transportation Research Board*, 2009, pp. 127–136.

[25] Wang, P. F., K. Wada, T. Akamatsu, and Y. Hara, An Empirical Analysis of Macroscopic Fundamental Diagrams for Sendai Road Networks. *Interdisciplinary Information Sciences*, Vol. 21, 2015, pp. 49–61.

[26] Ambühl, L., A. Loder, M. C. J. Bliemer, M. Menendez, and K. W. Axhausen, Introducing a re-sampling methodology for the estimation of empirical macroscopic fundamental diagrams. *Transportation Research Record: Journal of the Transportation Research Board*, , No. accepted, 2018.

[27] Ambühl, L., A. Loder, M. Bliemer, M. Menendez, and K. W. Axhausen, A functional form for the macroscopic fundamental diagram with a physical meaning. *Transportation Research Part B: Methodological*, Vol. In Press, 2018.

[28] Saeedmanesh, M. and N. Geroliminis, Clustering of heterogeneous networks with directional flows based on "Snake" similarities. *Transportation Research Part B: Methodological*, Vol. 91, 2016, pp. 250–269.

[29] Ji, Y., J. Luo, and N. Geroliminis, Empirical observations of congestion propagation and dynamic partitioning with probe data for large-scale systems. *Transportation Research Record: Journal of the Transportation Research Board*, Vol. 2422, 2014, pp. 1–11.

[30] Mazloumian, A., N. Geroliminis, and D. Helbing, The spatial variability of vehicle densities

as determinant of urban network capacity. *Philos Trans A Math Phys Eng Sci*, Vol. 368, No. 1928, 2010, pp. 4627–47.

[31] Berndt, D. J. and J. Clifford, Using dynamic time warping to find patterns in time series. In *Proceedings of the 3rd International Conference on Knowledge Discovery and Data Mining*, AAAI Press, 3000887, 1994, pp. 359–370.

[32] Sakoe, H. and S. Chiba, Dynamic programming algorithm optimization for spoken word recognition. *IEEE Transactions on Acoustics, Speech, and Signal Processing*, Vol. 26, No. 1, 1978, pp. 43–49.

[33] Alt, H. and M. Godau, Computing the Frechet distance between two polygonial curves. *International Journal of Computational Geometry Applications*, Vol. 05, No. 01n02, 1995, pp. 75–91.

[34] Toohey, K., *SimilarityMeasures: Trajectory Similarity Measures*, 2015, r package version 1.4.

[35] Aggarwal, C. C. and C. K. Reddy, *Data clustering: algorithms and applications*. Chapman and Hall/CRC, 2013.

[36] Kaufman, L. and P. Rousseeuw, Clustering by means of medoids. In *Statistical Data Analysis Based on the L_1 –Norm and Related Methods* (Y. Dodge, ed.), North-Holland, 1987, pp. 405–416.

[37] Vinod, H. D., Integer Programming and the Theory of Grouping. *Journal of the American Statistical Association*, Vol. 64, No. 326, 1969, pp. 506–519.

[38] Rousseeuw, P. J., Silhouettes: A graphical aid to the interpretation and validation of cluster analysis. *Journal of Computational and Applied Mathematics*, Vol. 20, 1987, pp. 53–65.

[39] Maechler, M., P. Rousseeuw, A. Struyf, M. Hubert, and K. Hornik, *cluster: Cluster Analysis Basics and Extensions*, 2018, r package version 2.0.7-1 — For new features, see the 'Changelog' file (in the package source).

[40] Gayah, V. V. and C. F. Daganzo, Clockwise hysteresis loops in the macroscopic fundamental diagram: An effect of network instability. *Transportation Research Part B: Methodological*, Vol. 45, 2011, pp. 643–655.

[41] Leclercq, L., N. Chiabaut, and B. Trinquier, Macroscopic fundamental diagrams: A cross-comparison of estimation methods. *Transportation Research Part B: Methodological*, Vol. 62, 2014, pp. 1–12.